



DOI: 10.19187/abc.20207272-82

Molecular Simulations Identify Target Receptor Kinases Bound by Astaxanthin to Induce Breast Cancer Cell Apoptosis

Mossa Gardaneh^{*a}, Zahra Nayeri^a, Parvin Akbari^a, Mahsa Gardaneh^b, Hasan Tahermansouri^c

^a Department of Stem Cells and Regenerative Medicine, Division of Medical Biotechnology, National Institute of Genetic Engineering and Biotechnology, Tehran, Iran

^b Department of Biology, York University, Toronto, Canada

^c Department of Chemistry, Ayatollah Amoli Branch, Islamic Azad University, Amol, Iran

ARTICLE INFO

Received:
17 May 2020
Revised:
23 May 2020
Accepted:
31 May 2020

Key words:
Breast cancer,
astaxanthin,
apoptosis,
receptor tyrosine kinase,

ABSTRACT

Background: We investigated molecular mechanisms behind astaxanthin-mediated induction of apoptosis in breast cancer cell lines toward combination therapy against cancer drug resistance.

Methods: Breast cancer cell lines were treated with serial concentrations of astaxanthin to determine its IC₅₀. We used drug-design software to predict interactions between astaxanthin and receptor tyrosine kinases or other key gene products involved in intracellular signaling pathways. Changes in gene expression were examined using RT-PCR. The effect of astaxanthin-nanocarbons combinations on cancer cells was also evaluated.

Results: Astaxanthin induced cell death in all three breast cancer cell lines was examined so that its IC₅₀ in two HER2-amplifying lines SKBR3 and BT-474 stood, respectively, at 36 and 37 μM ; however, this figure for MCF-7 was significantly lowered to 23 μM ($P < 0.05$). Astaxanthin-treated SKBR3 cells showed apoptotic death upon co-staining. Our *in silico* examinations showed that some growth-promoting molecules are strongly bound by astaxanthin via their specific amino acid residues with their binding energy standing below -6 KCal/Mol. Next, astaxanthin was combined with either graphene oxide or carboxylated multi-walled carbon nanotube, with the latter affecting SKBR cell survival more extensively than the former ($P < 0.05$). Finally, astaxanthin co-induced tumor suppressors p53 and PTEN but downregulated the expression of growth-inducing genes in treated cells.

Conclusions: These findings indicate astaxanthin carries' multitarget anti-tumorigenic capacities and introduce the compound as a suitable candidate for combination therapy regimens against cancer growth and drug resistance. Development of animal models to elucidate interactions between the compound and tumor microenvironment could be a major step forward towards the inclusion of astaxanthin in cancer therapy trials.

Introduction

Induction of cell death pathways constitutes the basis of cancer chemotherapy.¹ Drug resistance

particularly chemoresistance contributes to breast cancer (BC) recurrence post-surgery followed by secondary tumor formation and distant metastasis.² Natural compounds that can help chemo-sensitization of tumors without raising unwanted side effects have drawn attention for some time.^{3,4}

Astaxanthin (AST) is a red carotenoid pigment and a natural product of microalgae *Haematococcus pluvialis* with unique structural and chemical characteristics.⁵ AST is a powerful scavenger capable

Address for correspondence:

Mossa Gardaneh
National Institute of Genetic Engineering and Biotechnology,
Pazhoohesh Blvd, Tehran-Karaj HWY Kilometer 15,
PO BOX 14965/161, Tehran-Iran
Tel: +98 21 4458 0344
Fax: +98 21 4458-0395
Email: mossa65@nigeb.ac.ir, mossabenis65@yahoo.com



of degrading free radicals in aqueous solvents.⁶ It is a free oxygen inhibitor and an effective inhibitor of lipid peroxidation.⁷

Cancer incidence is rare among North American tribes who traditionally consume salmon fish (a rich source of AST).⁸ AST induces reduction of mouse tumor cells and synthesis of DNA.⁹ The compound also reduces mouse mammary tumor cells by 40%.¹⁰ Among eight carotenoids tested, AST most effectively inhibited the invasion of hepatoma cells.¹¹ AST inhibits growth among human cancer cell lines too. For example, two human colon cancer cell lines incubated with AST for 4 days lost their growth significantly compared to their controls.¹² The inhibiting effect of AST on human prostate cancer cells has also been reported.¹³ Finally, AST can prevent UV damage on DNA of skin fibroblasts, melanocytes and intestine cells.¹⁴

The anti-oxidant properties of AST restore superoxide dismutase (SOD) and catalase (CAT), thereby reducing intracellular O₂⁻ production and reversing lipopolysaccharide-induced toxicity and reactive oxygen species production in cancer cells.¹⁵ Such properties can also arrest cell cycle progression, inhibit cell proliferation and induce apoptosis by activating Nrf2-mediated anti-oxidant defense system.¹⁶ Unlike other carotenoids, there exists no report on the pro-oxidative properties of AST.

The anti-proliferative effects of AST on cancer cells of breast, liver and lung have been shown¹⁷ in parallel with a stronger growth inhibitory effect of AST compared to other carotenoids.¹⁶ Also, AST differentially affects cancer cells without harming normal ones.¹⁷ AST indeed protects wild-type cells against oxidative stress,^{18,19} ultraviolet,²⁰ neurotoxins,²¹ and cell-tissue inflammation²² via inhibiting apoptosis. In contrast, it forces cancer cells to commit apoptosis. AST-treated cancer cells show a significant peak of hypodiploid, indicative of apoptosis with typical characteristics including modified mitochondrial morphology, transmembrane potential and respiratory chain and regulated levels of *Bcl-2*, *Bax*, *Bad*, *Bcl-xL*.^{17,23}

In mouse models of cancer, the potential of AST in inducing apoptosis among tumor cells has been demonstrated. As an example, the compound inhibits tumorigenesis in rat colon via inducing apoptosis. AST can do this by controlling *ERK-2*, *AKT*, *MMPs-2/9*, *COX-2* and *NFκB* genes.²⁴ In another study, AST inhibited colon carcinogenesis by regulating inflammatory cytokines.²⁵ In hamster model of mouth cancer, dietary AST inhibited *NFκB* and *Wnt/β-catenin* by inhibiting *Erk/MAPK* and *PI3K/AKT*, eventually leading to apoptosis.²³ Based on its anti-inflammatory and anti-oxidant properties, AST was able to reduce proliferation and migration of BC cells compared to control normal breast epithelial cells.²⁶ The anti-invasive and anti-metastatic potential of AST has been shown in increasing metastasis-

specific miRNAs and suppressing the expression of *MYC* transcription factor.²⁷

In this study, we examined the effect of AST on the fate of BC cell lines and the changes it causes in expression levels of some key genes involved in BC cell tumorigenicity. We tested AST potential in binding to key growth signaling molecules including receptor tyrosine kinases, examined its impact on gene expression, and used nano particles to potentiate anti-tumorigenic effects of the carotenoid.

Methods

Cell culture

Three BC cell lines namely MCF-7, BT-474 and SKBR3 plus MCF-10, a breast epithelial line as a control, were obtained from the cell bank in NIGEB and fed with Dulbecco's Modified Eagle Medium (DMEM) supplemented with 10% FBS and incubated in 37 °C and 5% CO₂.

Cell treatment

To make a stock solution of AST, 53.1 mg of its powder (Santa Cruz Biotechnology Inc., USA) was dissolved in 9 mL DMEM and 1 mL DMSO to obtain a 10 mM solution. This solution was filtered and stored at -20 °C until use. The cells were seeded in 96-well plates with 5000-7000 cells per well in 100-150 μL medium and incubated for 24 hrs before treatment began. Serial dilutions of AST were added to the cells followed by cell incubation for 5 hrs. We used AST doses of 8, 16, 24, 36, 40, 50, 65, 80 μM and then tested cell viability in each cell line using the MTT Viability assay. Each dose was tested in triplicate wells for each cell line and the whole experiment was repeated three times. Due to the lethal properties of DMSO as a solvent, and to determine AST independent effect, the cells were also treated with DMSO for the equivalent volumes in parallel.

Cell death analyses

We used MTT assay to measure cell viability as a percentage of untreated WT control cells. Briefly, a 5-mg/mL stock of MTT solution in PBS was formed from which 20 μL was added to 80 μL cell medium in each well of 96-well plates and incubated for 4 hrs. The medium was then replaced with 100 μL DMSO for another 30-min shaking-incubation at dark before reading absorbance in 580 nM (excitation) and 620 nM (emission) using an ELISA reader. An average of the produced figures in various doses of AST was used to determine AST effective dose.

Cell co-staining and live cell count

Since acridine orange (AO) co-applied with ethidium bromide (EB) stains nuclear DNA green in live cells and orange in dead cells, we followed the standard co-staining method to measure the percentage of viable SKBR3 cells. Cell groups were



suspended at a normal counting concentration from which 50 μ L was mixed with 50 μ L of the stain in 96-well plates and subjected to counting under fluorescent light. Images were captured using a fluorescence microscope coupled with a Nikon digital camera. Six random microscopic fields per well were selected to count an average of 120 cells counted for each cell group in triplicates (three wells per group). Green cells and orange cells were considered, respectively, as living and dead cells. The data collected from three independent experiments were then expressed as the percentage of living cells by dividing the number of living cells by the number of total cells counted (living + dead).

Bioinformatic analysis of astaxanthin interactions with target molecules

Three classes of luminal B, HER2⁺ and basal like/triple negative are considered as the main subtypes in BC. First, we used KEGG (Kyoto Encyclopedia of Genes and Genomes) database to identify molecular pathways involved in BC tumorigenesis. In this database, diseases are considered as induced molecular network systems. The aim of using this database was to reach a common signaling pathway among BC subtypes and, therefore, to reach therapeutic aims and target proteins. The next step was to determine the structure of selected proteins from Protein Data Bank (www.rcsb.org).

In order to prepare protein structures, we used the AutoDockTools software (<http://autodock.scripps.edu/resources/adt>). We omitted ligands and water molecules from the structure of each protein without deleting cofactors. The AST structure was captured

from Chempidder (<http://www.chemspider.com/>) and ATB site developed by the University of Queensland, Australia (<https://atb.uq.edu.au>) was utilized to design and optimize the AST molecular structure. We ultimately examined molecular docking using AutoDockTools. In this procedure, we first converted pdb files of ligands and proteins to pdbqt. Then, we applied the AutoGrid program in order to obtain a map for docking simulation. To do this, after defining proteins and ligands, Grid box in the active site of each protein was adjusted. In the next step, AutoDock was used for simulation using genetic algorithm as the searching parameter. In order to obtain dock scores, the docking protocol used in the study consisted of 200 independent runs along with population size=150 and the Lamarckian genetic algorithm was applied for all docking runs reported in Kcal/mol. Finally, the figures of interactions between AST and the selected proteins were portrayed through Discovery Studio Visualization software.

Reverse transcription (RT) PCR

RT-PCR was carried out as reported.²⁸ Briefly, total RNA was extracted, DNase treated, and used (2 μ g) for cDNA synthesis. To amplify target DNA fragments, the cDNA samples were first denatured at 95 °C for 2 min before amplification. Table 1 shows the primer pairs we used for each gene candidate. PCR reactions were carried out for 30 cycles consisting of denaturation at 95 °C for 45", annealing at various temperatures. Gel electrophoresis and band intensity measurements were duplicated as reported.²⁸

Table 1. Primer sequences for RT-PCR

Name	Primer Sequence	Size (bp)	Anneal. Temp	Accession #
EGFR	F TCCTTTGGAAAACCTGCAGA R TGCTCTCCACGTTGCACA	188	52.2°C × 20"	NM_005228.5
PTEN	F CAATTCAGGACCCACACGAC R CCTCTGGTCTGGTATGAAGA	173	53.2°C × 20"	NM_000314.7
IGF1R	F CTTGTGAAGTCTTGCCC R GAGCCCCATGAAGTTCTCCA	225	53°C × 20"	NM_000875.5
AKT1	F AGGATGTGGACCAACGTGAG R GTGCGTTCGATGACAGTGG	133	54.2°C × 20"	NM_005163.2
AKT2	F CATCAAAGAAGGCTGGCTCC R ACGGAGAAGTTGTTAAGGGG	153	53.8°C × 60"	NM_001626.6
ERK1	F ATCAGCCCCTTCGAACATCA R ACAGGTCAGTCTCCATCAGG	172	52°C × 20"	NM_002746.3
ERK2	F ACATTCAACCCACACAAGAGG R TCGAACTTGAATGGTGCTTCG	254	53.4°C × 60"	NM_002745.4
P53	F CCCCTCCTGGCCCCTGTCATCTTC R GCAGCGCCTCACAACCTCCGTCAT	265	54.8 °C × 60"	NM_001126118.1
GAPDH	F GTCTCCTCTGACTTCAACAGCG R GTCTCCTCTGACTTCAACAGCG	130	56°C × 60"	NM_002046



Combination of astaxanthin and carbon nanomaterials

Two carbon nanomaterials were used to combine with AST: graphene oxide (GO) and carboxylated multi-walled carbon nanotube (MWCNT-COOH). Their characteristics were as follows:

1. MWCNT-COOH: %95 purity, OD: 10-30 nm, Length: 0.5-2 μm , Neutrino Co., Ltd.
2. GO nanoplatelets (99%, Thickness 3.4-7 nm with 6-10 Layers).

The concentration of AST was performed by Unico UV-2100 Model variable-wavelength UV-Vis spectrophotometry. Field emission scanning electron microscope (FESEM) was taken using an MIRA3\TESCAN-XMU model. Fourier transform infrared spectroscopy (FT-IR) was recorded using KBr tablets on a Thermo Nicolet Nexus 870 FTIR spectrometer.

In order to load AST on nanotubes, 30 mg of GO or MWCNT-COOH was dispersed into 15 mL ethanol containing 100 mg/L of AST for 4 h. The amounts of absorbed AST were calculated as the difference between the initial and final concentrations when the equilibrium was reached. After 4h, the AST concentration in the aqueous solutions was determined by UV-Vis spectroscopy. The adsorption (%) was obtained as follows:

$$\% \text{ Adsorption} = \frac{C_0 - C_e}{C_0} \times 100$$

where C_0 and C_e are, respectively, the initial and

final concentrations (mg/L) of AST in the aqueous solution.

Statistical analyses

Data in the figures are represented as the mean \pm standard error of the mean (SEM) of three or more separate experiments. Student's T-test was used to analyze differences between two groups. Differences among three or more groups were analyzed by one-way analysis of variance (ANOVA), followed by a post hoc Duncan Multiple-comparisons Test ($P < 0.05$, statistically significant; $P < 0.01$, highly significant).

Results

Death induction in breast cancer cell lines by astaxanthin

We measured viability of AST-treated BC cell lines and found that the compound kills the cells at its lethal dose within 5 hours of treatment. Our results showed that IC₅₀s for BT-474, SKBR3 and MCF-7 are, respectively, 36, 37 and 23 μM with no significant effect on normal controls MCF-10 (Figure 1). We also found that the cell death is dose dependent and accelerated beyond a range of the drug dose (Fig. 1B-D).

Morphological changes towards apoptosis post-treatment with astaxanthin

Cell co-staining using acridine orange and ethidium bromide reveals altered morphologies typical of apoptosis among cell samples (Figure 2). Over 29% of SKBR3 cells treated with 36 μM AST

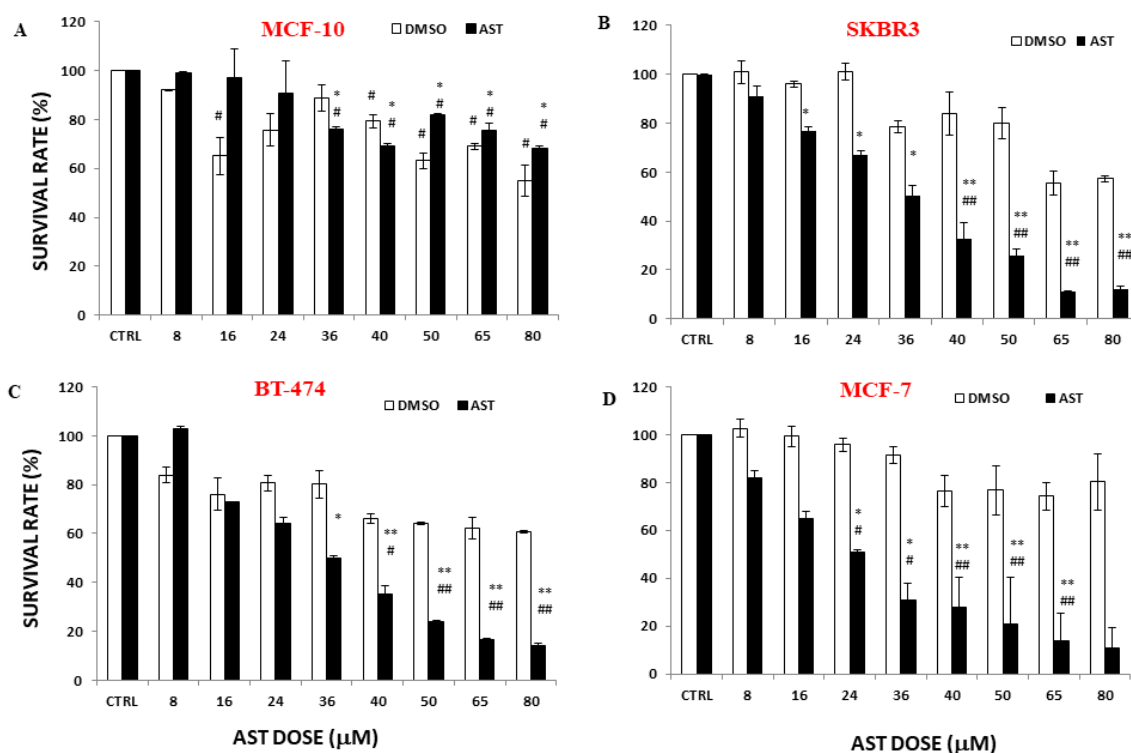


Figure 1. The effect of astaxanthin on survival of breast cancer cell lines. Each column represents an average of three independent experiment carries out in triplicates. Symbols * and ** indicate statistical differences between each column with its counterpart in control, whereas symbols # and ## show differences between each column of AST-treated cells and its control treated with DMSO.

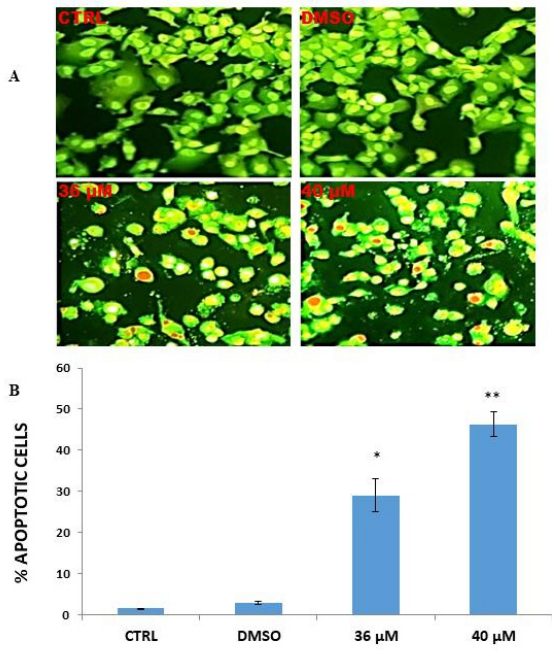


Figure 2. Apoptotic death amongst SKBR3 cells treated with two astaxanthin doses. Each column represents an average of three independent experiments carries out in triplicates by random counting of microscopic fields as detailed in Methods. Symbols * and ** indicate statistical differences between each column with its control counterpart.

underwent apoptosis compared to their untreated controls ($P < 0.05$), whereas this rate increased to 46% in the presence of 40 μM AST ($P < 0.01$).

Strong binding between astaxanthin and key intracellular molecules

The KEGG database encompasses data of genomics, biological pathways, human diseases, drugs and chemicals (Figure 3.1). The KEGG pathway analysis introduced PI3K/AKT and MAPK/ERK as the common signaling pathways that are actively present in all BC subtypes, hence their targeting can be translated to control all BC subgroups. To perform the docking studies, the following protein structures were captured from Protein Data Bank (PDB): AKT1 (1UNQ) and AKT2 (1O6L) as key proteins involved in the PI3K/AKT pathway, IGFR (5FXS) and EGFR (2RGP) as common receptors involved in cancer development, and ERK1 (4QTB) and ERK2 (3SA0) as principal proteins included in the MAPK/ERK pathway (Figure 3.2).

Following the preparation of ligands and proteins, docking was carried out in order to simulate drug-

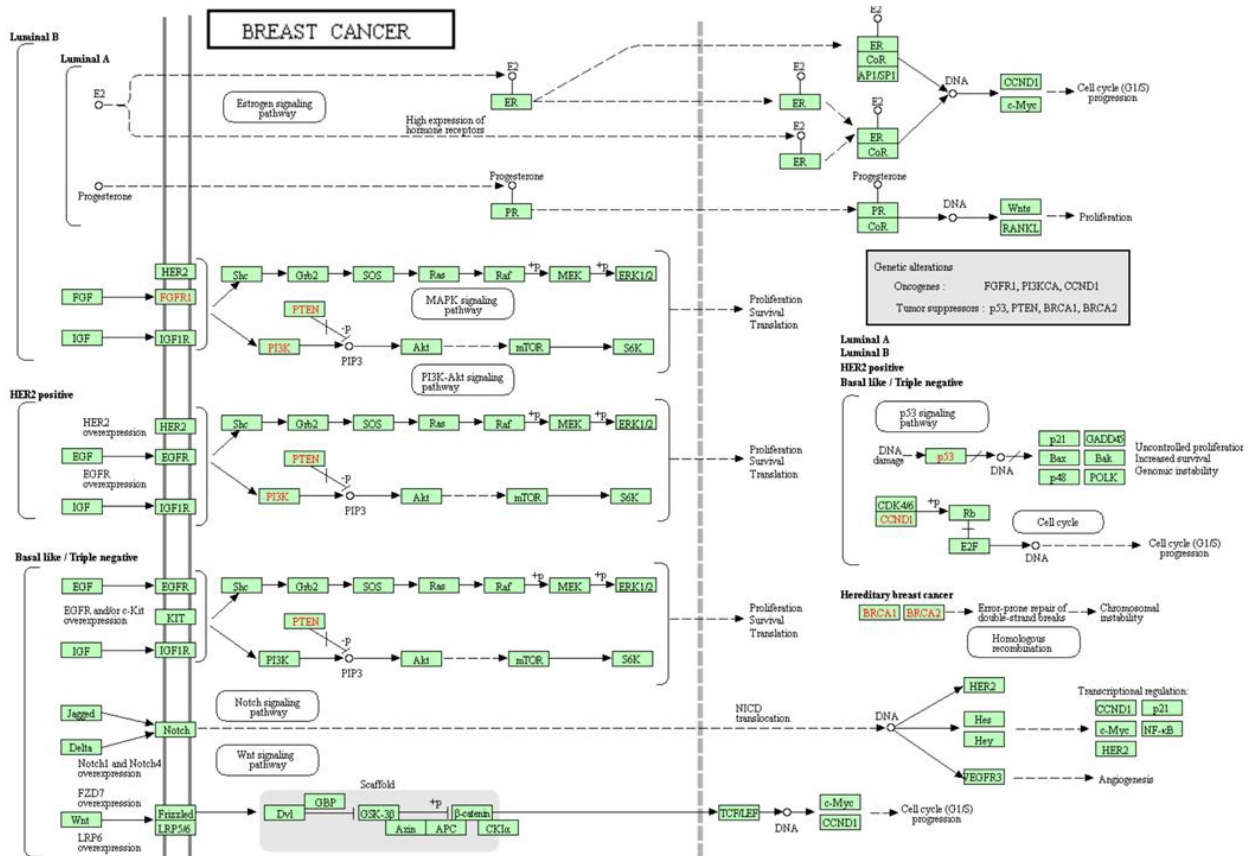


Figure 3.1. The KEGG database representing molecular pathways involved in breast cancer tumorigenesis.

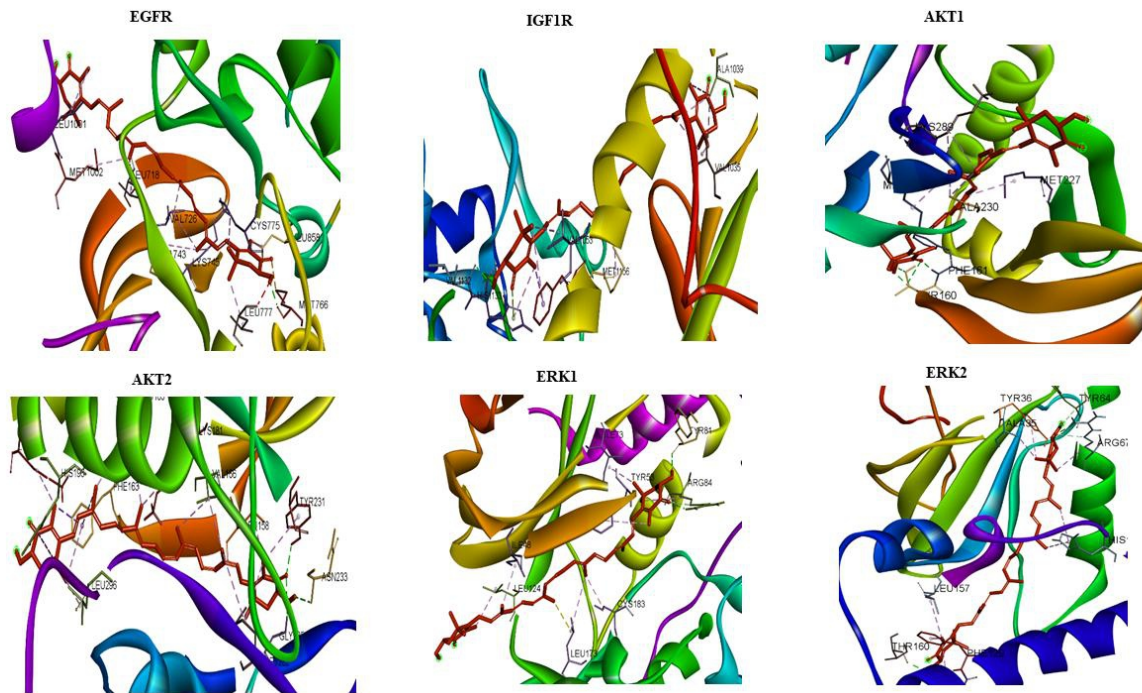


Figure 3.2. Astaxanthin reaction with a number of cell growth pathway proteins. See text for details.

receptors bindings. Table 2 shows the information related to five conformers with the least binding energy for each protein. These results indicate that AST can strongly bind to each of these proteins via their specific amino acid residues, leading to their inhibition.

Simulation by docking showed that the lowest binding energies of AST with AKT1 and AKT2 were -8.49 and -10.69 between, respectively, two amino acids THR160, PHE161 in AKT1 and three amino acids GLY235, TYR231 and ASN233 within AKT2. IGF1R with -11.37 and EGFR with -9.48 binding energies form an H bond with AST in, respectively, amino acids VAL1132 and MET766. Finally, AST interaction with ERK1/2 shows binding energies of -10.38 and -11 involving, respectively, amino acids TRY81, ARG84 in ERK1 and THR160, ARG67 in ERK2 (Figure 3). We also tested AST binding to various sites in random within the CD44 receptor protein but did not find favorable binding sites in the receptor structure.

Altered expression of growth signaling genes in astaxanthin-treated SKBR3 cell line

Table 2. Binding energy for 5 initial conformers of target proteins.

Protein	Lowest Binding Energy (KCal/mol)
AKT1	-8.49
AKT2	-10.69
ERK1	-10.38
ERK2	-11.00
IGF1R	-11.37
EGFR	-9.48

Changes in mRNA expression of genes involved in growth pathways and tumor suppressor gene PTEN were monitored in SKBR3 cells. As shown in Figure 4, expression of RTKs, EGRF and IGF1R, and other cell growth-promoting genes AKT1, AKT2, ERK1 and ERK2 was reduced upon AST treatment of the cells and most of these changes were statistically significant compared to untreated controls (Fig. 4; $P < 0.01$). In contrast, the expression of tumor suppressors p53 and PTEN that promote apoptosis against cell growth, significantly increased upon AST treatment ($P < 0.01$).

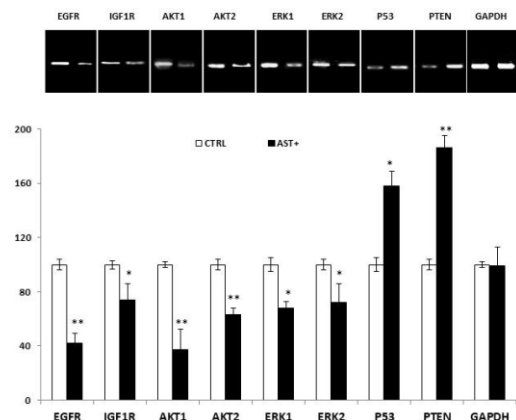


Figure 4. Altered expression of key genes under astaxanthin treatment. The gel image shows RT-PCR products. The intensity of the gel bands was measured as outlined in Methods to produce the graph. Each column in the graph represents two independent RT-PCR experiments. Symbols * and ** show statistical differences between each column and its control counterpart.

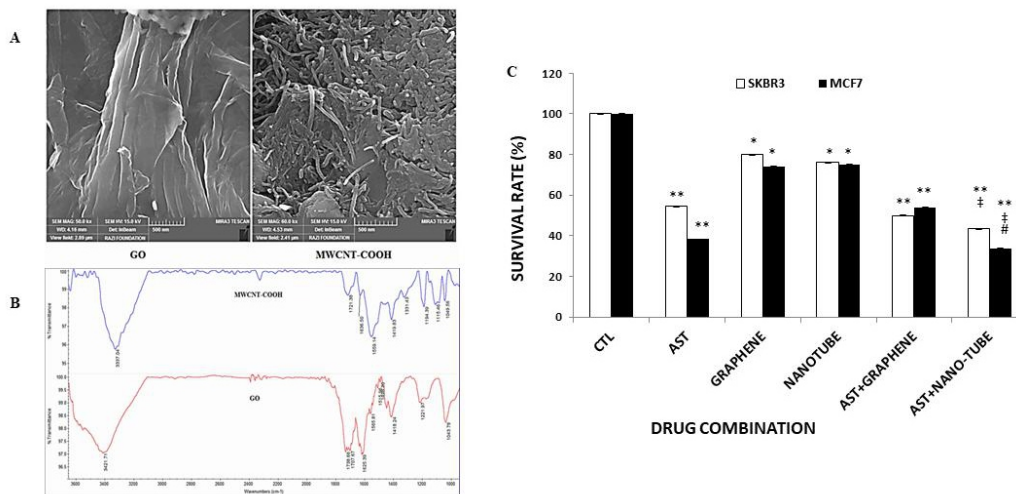


Figure 5. Acceleration of BC cell death treated with nano-astaxanthin compounds. The two images on the left show electron microscopy and adsorption spectroscopy, respectively. The right graph shows survival of treated BC cells. Each column represents an average of three independent experiments carried out in triplicates by random counting of microscopic fields as detailed in Methods. Symbols * and ** indicate statistical differences between each column with its control counterpart, whereas symbol ‡ shows difference between nano-AST and AST alone and symbol # shows differences between nano-AST and nano particle control.

Acceleration of SKBR3 cell death using nano-astaxanthin

Figure 5 shows Field Emission Scanning Electron Microscope (FESEM) images and Fourier Transform InfraRed (FT-IR) spectroscopy of GO and MWCNT-COOH. FESEM images of GO and MWCNT-COOH were presented in Figure 5A. It is evident from these images that GO sheets illustrate the sheet-like structure with large thickness, smooth surface, and wrinkled edge. In addition, FESEM image of MWCNT-COOH shows that MWCNTs are curved, rope-like and highly tangled and agglomerated with each other. These results clearly confirm the morphology of MWCNT-COOH and GO.

The chemical structures of GO and MWCNT-COOH were determined by FT-IR analysis as presented in Figure 5B. In this figure, the peaks at 1700-1735 (C=O) and 1000-1200 (C-O) cm^{-1} are assigned to the C=O stretching vibration and C-O stretching mode which clearly shows carboxylic groups on the MWCNT-COOH and GO. In addition, the absorption peaks at 3300-3500 and 1500-1640 cm^{-1} obviously indicating stretching vibration of hydroxyl groups and the C=C vibration, respectively. These results show that plenty of hydroxyl and carboxyl groups were located on both carbon materials, particularly on GO.

On this basis, the adsorption percentage by GO and MWCNT-COOH was calculated to be 68% and 93%, respectively. This shows that MWCNT-COOH has significantly adsorbed AST in comparison to GO. Since AST is an almost non-polar molecule, π - π interactions play important roles in its adsorption process. On the other hand, the abundant polar groups in GO cause less adsorption of GO than MWCNT-COOH.

After producing our nano-drugs, cancer cell lines

SKBR3 and MCF-7 were treated, respectively, with 20 and 24 μM AST alone or nano-AST compounds. As shown in Fig. (5C), the percentage of the cells killed by GO-AST was comparable to the percentage of those killed by AST alone. However, the combination of AST+MWCNT-COOH accelerated cell death in both lines so that the difference with those under AST alone became significant (Figure 5C; $P < 0.05$). Also, MCF-7 cells suffered more death than SKBR3 lines after treatment with AST+MWCNT-COOH ($P < 0.05$).

Discussion

In this study, we showed that AST significantly reduces viability and induces apoptosis in three different BC cell lines. Based on the levels of *HER2* we have previously detected in these cell lines²⁹, it is conceivable from our current data that AST impact on cell survival might conversely correlate with *HER2* content.

According to the KEGG database, several key molecules are involved in the cells' survival and growth; therefore, among them, we selected EGFR, IGF1R, AKT, ERK1/2, and PTEN for analysis. Our data in silico indicated strong binding of AST to these molecules. These observations primarily suggest that although *HER2* is a determinant receptor in cancer cell growth, AST binding to alternative molecules on the row may eventually overcome *HER2* pro-growth function by providing a bypassing route toward disruption of growth signals. This might explain the reduced levels of viability among *HER2*-amplifying BC cell lines upon receiving higher doses of AST.

The strong binding of AST to key RTKs and downstream molecules also indicates the unexplored anti-neoplastic capacity of the photochemical compound. Overexpression or dysfunction of EGFR



(HER1 in humans) due to mutations plays a role in tumorigenesis.³⁰ Ligand binding can activate EGFR molecules to homo- or hetero-dimerize with HER2³¹ or another EGFR member and these changes induce EGFR auto-phosphorylation in several of its tyrosine residues. These changes initiate downstream signaling pathways including MAPK, AKT and JNK, leading to DNA synthesis and cell proliferation³² plus cell migration. Conversely, inhibition of EGFR signaling may inhibit tumor formation or growth. Inhibitors of the EGFR oncogene have been developed against various cancer types that include several small molecules and antibodies e.g. gefitinib. However, the use of these therapeutics is likely to cause resistance in cancer cells through increasing the activity of key molecules such as STAT3.³³

We showed that beside EGFR, AST also strongly binds the insulin-like growth factor 1 (IGF-1) receptor (IGF1R). This receptor promotes cell growth by interacting IGF-1 and IGF-2, and IGF1R amplification and/or overexpression has implications in chemo- and radio-resistance and metastasis in several cancer types including BC.^{34,35} Indeed, triple-negative BC (TNBC) cells overexpress IGF1R at considerable levels, leading to elevated proliferation, aggressive subtypes, and survival of all TNBCs.³⁶ Cross-talks between EGFR and IGF1R prevent EGFR inhibitors from activity and so allow EGFR signaling to resume in the presence of these inhibitors. Our analysis *in silico* indicated that AST can strongly bind to a number of amino acid residues in these molecules. Simultaneous inhibition of EGFR and IGF1R by AST indicates the potential of the compound in blocking EGFR-IGF1R cross-talks and bypassing drug resistance caused upon utilizing inhibitors. Therefore, the anti-tumorigenic potency of the compound can be explored along with chemical inhibitors or chemotherapy drugs against BC.

In addition to inhibitory binding to key molecules of the common cell growth pathways, AST treatment also induced mRNA expression of p53 in our SKBR3 cells. Similar to hepatoma and colon cancer.^{37,38} AST-mediated dose-dependent induction of phospho-p53 leading to induced cell cycle arrest and enhanced apoptosis has been shown in BC lines MCF-7 with wild-type p53 and MDA-MB-231 that carries mutant p53.³⁹ P53 can act as both an oncogene and a tumor suppressor so that its mutations are largely translated to tumor aggression, whereas its restoration leads to tumor regression. AST-mediated induction of p53 expression adds to the multitarget potential of the carotenoid against tumorigenesis, with its therapeutic benefits exceeding those of the anti-cancer dexamethasone.⁴⁰ An extension of our study would examine how changes in p53 mRNA levels correlate with alterations in protein levels and activity.

Astaxanthin further downregulated the expression of Phosphatase and Tensin Homolog (PTEN). The

PTEN tumor suppressor gene, via its phosphatase activity, plays a role in cell cycle regulation and prevents cells from overgrowth and rapid division.⁴¹ The phosphatase activity of PTEN preferentially dephosphorylates PIP3 and so results in the inhibition of the AKT/PKB signaling pathway that regulates cell growth, survival, and migration.^{42,43} Conversely, PTEN mutations contribute to the development of many cancers, with loss of PTEN tumor suppressor commonly occurring in human cancer particularly in prostate cancer⁴⁴ and reduction of its expression in BC.⁴⁵ These add to the importance of PTEN induction by AST as an anti-tumor measure.

PTEN interacts with p53 to regulate EMT and cell migration.⁴⁶ Our study on SKBR3 cells showed that AST induces p53 expression and, in parallel, restores lost levels of PTEN. *In vivo* studies using patient-derived xenograft HER2 models of BC similar to what we have developed before²⁹ could provide deeper insights into the ultimate impact of PTEN-p53 co-induction by AST on HER2⁺ BC tumor growth and outcome.

In fact, combined versus individual disruption of p53 and PTEN induces TNBC growth with clear activating impact on PI3K/AKT signaling, changes that lead to distinct mesenchymal features and poor clinical outcome.⁴⁷ Compared to the wild-type p53 expressed in MCF-7⁴⁸, MDA-MB-231 carries mutant p53, which confers survival advantage to the TNBC cell line by suppressing apoptosis.⁴⁹ Due to these differences, higher doses of AST are needed to kill MDA-MB-231 cells.³⁹ If applied in TNBC line MDA-MB-231 and therapy-resistant TNBC tumor models carrying either wild-type or mutant p53, our *in silico* strategy might shed more light on the impact of PTEN-p53 interactions, upon AST treatment, on cancer cell growth and ultimately on tumor fate.

In conclusion, our *in silico* experiments showed that AST promotes induction of apoptotic cell death by interactions with key genes of tumorigenesis. When combined with nanotubes, the cell death rate amongst cancer cells increases significantly, an important development in breaking drug resistance in BC tumors. These anti-tumorigenic effects of AST provide a glimpse of a global picture of the effect of phytochemicals on BC therapy and/or prevention. Animal studies focusing on AST and nano-AST-mediated changes in expression of tumor suppressors, RTKs and growth pathway molecules as well as AST interactions with anti-metastatic miRNAs will consolidate our findings in the actual tumor cells and tumor microenvironment and assess AST utilities against tumor chemoresistance and metastasis in combined modes of clinical BC therapy.

Acknowledgement

This study was funded by a grant (541) from National Institute of Genetic Engineering and



Biotechnology (NIGEB) in Tehran, Iran. The authors thank all colleagues and students who assisted us in completing this study.

Conflict of Interest

The authors declare no conflict of interest.

References

1. Zheng HC. The molecular mechanisms of chemoresistance in cancers. *Oncotarget*. 2017; 8:59950-59964, doi:10.18632/oncotarget.19048
2. Chuthapisith S, Eremin J, El-Sheemey M, Eremin O. Breast cancer chemoresistance: emerging importance of cancer stem cells. *Surg Oncol*. 2009; 19:27-32
3. Turrini E, Ferruzzi L, Fimognari C. Natural compounds to overcome cancer chemoresistance: toxicological and clinical issues. *Expert Opin Drug Metab Toxicol*. 2014; 10:1677-90.
4. Wang P, Li H, Yang YJ, Wang L, Lee SC. Overcome Cancer Cell Drug Resistance Using Natural Products. *Evidence-Based Complement Alternat Med*. 2015; 767136.
5. Guerin M, Huntley ME, Olaizola M. Haematococcus astaxanthin: applications for human health and nutrition. *Trends Biotechnol*. 2003; 21:210-216
6. Bagchi D, Garg A, Krohn RL, Bagchi M, Tran MX, Stohs SJ. Oxygen free radical scavenging abilities of vitamins C, E, β -carotene, pycnogenol, grape seed proanthocyanidin extract and astaxanthins in vitro. *Res Commun Mol Pathol Pharmacol*. 2001; 95:179-189
7. Naguib YM. Antioxidant activities of astaxanthin and related carotenoids. *Agri Food Chem*. 2000; 48:1150-1154
8. Bates C, Van Dam C, Horrobin DF, Morse N, Huang YS, Manku MS. Plasma essential fatty acids in pure and mixed-race American Indians on and off a diet exceptionally rich in salmon. *Prostaglandins Leukot Med*. 1985; 17:77-84
9. Sun S, Gross MD, Iijima K, Jyonouchi H. Anti-tumor activity of astaxanthin on Meth-A tumor cells and its mode of action. *FASEB J*. 1998; 12:966-966
10. Kim HW, Park JS, Chew BP. B-carotene and astaxanthin inhibit mammary tumor cell growth and induce apoptosis in mice in vitro *FASEB J*. 2001; 15:298-298
11. Kozuki Y, Miura Y, Yagasaki K. Inhibitory effects of carotenoids on the invasion of rat ascites hepatoma cells in culture. *Cancer Lett*. 2000; 151:111-115
12. Onogi N, Okuno M, Matsushima-Nishiwaki R, Fukutomi Y, Moriwaki H, Muto Y, Kojima S. Antiproliferative effect of carotenoids on human colon cancer cells without conversion to retinoic acid. *Nutr Cancer*. 1998; 32:20-24
13. Ni X, Yu H, Wang S, Zhang C, & Shen S. Astaxanthin Inhibits PC-3 Xenograft Prostate Tumor Growth in Nude Mice. *Mar Drugs*. 2017; 15:66
14. Lyons NM, O'Brien NM. Modulatory effects of an algal extract containing astaxanthin on UVA-irradiated cells in culture. *J Dermatol Sci*. 2002; 30:73-84
15. Franceschelli S, Pesce M, Ferrone A, de Lutiis MA, Patruno A, Grilli A, *et al*. Astaxanthin treatment confers protection against oxidative stress in U937 cells stimulated with lipopolysaccharide reducing O₂- production. *PLoS ONE*, 2014; 9:e88359.
16. Zhang X, Zhao WE, Hu L, Zhao L, Huang J. Carotenoids inhibit proliferation and regulate expression of peroxisome proliferators-activated receptor gamma (PPARgamma) in K562 cancer cells. *Arch Biochem Biophys*. 2011; 512:96-106
17. Song XD, Zhang JJ, Wang MR, Liu WB, Gu XB, Lv CJ. Astaxanthin induces mitochondria-mediated apoptosis in rat hepatocellular carcinoma CBRH-7919 cells. *Bullet Pharmaceut Bullet*. 2011; 34:839-844
18. Dong LY, Jin J, Lu G, Kang XL. Astaxanthin attenuates the apoptosis of retinal ganglion cells in db/db mice by inhibition of oxidative stress. *Marine Drugs*. 2013; 11:960-974
19. Song X, Wang B, Lin S, Jing L, Mao C, Xu P, Lv C, Liu W, Zuo J. Astaxanthin inhibits apoptosis in alveolar epithelial cells type II in vivo and in vitro through the ROS-dependent mitochondrial signaling pathway. *J Cell Mol Med*. 2014; 18:2198-2212
20. Hama S, Takahashi K, Inai Y, Sakamoto R, Yamada A, Tsuchiya H, Kanamura K, Yamashita E, Kogure K. Protective effects of topical application of a poorly soluble antioxidant astaxanthin liposomal formulation on ultraviolet-induced skin damage. *J Pharmacol Sci*. 2012; 101(8):2909-16
21. Ye Q, Huang B, Zhang X, Zhu Y, Chen X. Astaxanthin protects against MPP⁺-induced oxidative stress in PC12 cells via the HO-1/NOX2 axis. *BMC Neurosci*. 2012; 13:156
22. Kim YJ, Kim YA, Yokozawa T. Protection against oxidative stress, inflammation, and apoptosis of high-glucose-exposed proximal tubular epithelial cells by astaxanthin. *J Agric Food Chem*. 2009; 57:8793-8797
23. Kavitha K, Kowshik J, Kishore TK, Baba AB, Nagini S. Astaxanthin inhibits NF- κ B and Wnt/ β -catenin signaling pathways via inactivation of Erk/MAPK and PI3K/Akt to induce intrinsic apoptosis in a hamster model of oral cancer. *Biochimica et Biophysica Acta (BBA) - General Subjects*. 2013; 1830:4433-4444
24. Nagendraprabhu P, Sudhandiran G. Astaxanthin inhibits tumor invasion by decreasing extracellular



- matrix production and induces apoptosis in experimental rat colon carcinogenesis by modulating the expressions of ERK-2, NFkB and COX-2. *Invest New Drugs*. 2011; 29:207-224
25. Yasui Y, Hosokawa M, Mikami N, Miyashita K, Tanaka T. Dietary astaxanthin inhibits colitis and colitis-associated colon carcinogenesis in mice via modulation of the inflammatory cytokines. *Chem Biol Interact*. 2011; 193:79-87
 26. McCall B, McPartland CK, Moore R, Frank-Kamenetskii A, Booth BW. Effects of Astaxanthin on the Proliferation and Migration of Breast Cancer Cells In Vitro. *Antioxidants (Basel)*. 2018; 7(10):135
 27. Kim HY, Kim YM, Hong S. Astaxanthin suppresses the metastasis of colon cancer by inhibiting the MYC-mediated downregulation of microRNA-29a-3p and microRNA-200a. *Sci Rep*. 2019; 9(1):9457
 28. Gardaneh M, Gholami M, Maghsoudi N. Synergy between glutathione peroxidase-1 and astrocytic growth factors suppresses free radical generation and protects dopaminergic neurons against 6-Hydroxydopamine. *Rejuven Res*. 2011; 14:195-204
 29. Gardaneh M, Shojaei S, Kaviani A, Behnam B. GDNF induces RET-SRC-HER2-dependent growth in trastuzumab-sensitive but SRC-independent growth in resistant breast tumor cells. *Breast Cancer Res Treat*. 2017; 162(2):231-241
 30. Zhang H, Berezov A, Wang Q, Zhang G, Drebin J, Murali R, Greene MI. ErbB receptors: from oncogenes to targeted cancer treatment. *J Clin Invest*. 2007; 117:2051-8
 31. Wieduwilt MJ, Moasser MM. The epidermal growth factor receptor family: biology driving targeted therapeutics. *Cell Mol Life Sci*. 2008; 65(10):1566-84
 32. Oda K, Matsuoka Y, Funahashi A, Kitano H. A comprehensive pathway map of epidermal growth factor receptor signaling. *Mol Systems Biol*. 2005; 1:2005.0010
 33. Wen W, Wu J, Liu L, Tian Y, Buettner R, Hsieh MY, Home D, Dellinger TH, Han ES, Jove R, Yim JH. Synergistic anti-tumor effect of combined inhibition of EGFR and JAK/STAT3 pathways in human ovarian cancer. *Mol Cancer*. 2015; 14(1):100
 34. Denduluri SK, Idowu O, Wang Z, Liao Z, Yan Z, Mohammed MK, Ye J, Wei Q, Wang J, Zhao L, Luu HH. Insulin-like growth factor (IGF) signaling in tumorigenesis and the development of cancer drug resistance. *Genes Dis*. 2015; 2(1):13-25, 2015
 35. Brahmkhatri VP, Prasanna C, Atreya HS. Insulin-like growth factor system in cancer: novel targeted therapies. *Biomed Res Int*. 2015; 538019
 36. Soljic M, Mrklic I, Tomic S, Omrcen T, Sutalo N, Bevanda M, Vrdoljak E. Prognostic value of vitamin D receptor and insulin-like growth factor receptor 1 expression in triple-negative breast cancer. *J Clin Pathol*. 2018; 71(1):34-9
 37. Liu X, Song M, Gao Z, Cai X, Dixon W, Chen X, Cao Y, Xiao H. Stereoisomers of astaxanthin inhibit human colon cancer cell growth by inducing G2/M cell cycle arrest and apoptosis. *J Agr Food Chem*. 2016; 64(41):7750-7759
 38. Messina CM, Manuguerra S, Renda G, Santulli A. Biotechnological Applications for the Sustainable Use of Marine By-products: In Vitro Antioxidant and Pro-apoptotic Effects of Astaxanthin Extracted with Supercritical CO₂ from *Parapeneus longirostris*. *Marine Biotech*. 2019; 1-12.
 39. Sowmya PR, Arathi BP, Vijay K, Baskaran V, Lakshminarayana R. Astaxanthin from shrimp efficiently modulates oxidative stress and allied cell death progression in MCF-7 cells treated synergistically with beta-carotene and lutein from greens. *Food Chem Toxicol*. 2017; 106(Pt A):58-69
 40. Wang M, Zhang J, Song X, Liu W, Zhang L, Wang X, Lv C. Astaxanthin ameliorates lung fibrosis in vivo and in vitro by preventing transdifferentiation, inhibiting proliferation, and promoting apoptosis of activated cells. *Food Chem Toxicol*. 2013; 56:450-458
 41. Jerde TJ. Phosphatase and tensin homologue: novel regulation by developmental signaling. *J Sign Transduct*. 2015; 282567.
 42. Leslie NR, Downes CP. PTEN function: how normal cells control it and tumour cells lose it. *Biochem J*. 2004; 382(Pt 1):1-11
 43. Hopkins BD, Hodakoski C, Barrows D, Mense SM & Parsons, RE. PTEN function: the long and the short of it. *Trends Biochem Sci*. 2014; 39(4):183-90
 44. Jamaspishvili T, Berman DM, Ross AE, Scher HI, De Marzo AM, Squire JA, Lotan TL. Clinical implications of PTEN loss in prostate cancer. *Nat Rev Urol*. 2018; 15(4):222-234
 45. Zhang HY, Liang F, Jia ZL, Song ST & Jiang ZF. PTEN mutation, methylation and expression in breast cancer patients. *Oncol Lett*. 2013; 6(1):161-168
 46. Martin P, Liu YN, Pierce R, Abou-Kheir W, Casey O, Seng V, Camacho D, Simpson RM, Kelly K. Prostate epithelial Pten/TP53 loss leads to transformation of multipotential progenitors and epithelial to mesenchymal transition. *Am J Pathol*. 2011; 179(1):422-435
 47. Liu JC, Voisin V, Wang S, Wang DY, Jones RA, Datti A, Uehling D, Al-awar R, Egan SE, Bader GD, Tsao M, Mak TW, Zacksenhaus E. Combined deletion of Pten and p53 in mammary epithelium accelerates triple-negative breast



- epithelium accelerates triple-negative breast cancer with dependency on eEF2K. *EMBO Mol Med.* 2014; 6(12):1542–1560
48. Lu X, Errington J, Curtin NJ, Lunec J, Newell DR. The impact of p53 status on cellular sensitivity to antifolate drugs. *Clin Cancer Res.* 2001; 7:2114–2123
49. Hui L, Zheng Y, Yan Y, Bargonetti J, Foster DA. Mutant p53 in MDA-MB-231 breast cancer cells is stabilized by elevated phospholipase D activity and contributes to survival signals generated by phospholipase D. *Oncogene.* 2006; 25:7305–10